JCIM JOURNAL OF CHEMICAL INFORMATION AND MODELING

pubs.acs.org/jcim Article

Umbrella Sampling Simulations of Cardiac Thin Filament Reveal Thermodynamic Consequences of Troponin I Inhibitory Peptide Mutations

Austin M. Cool and Steffen Lindert*

Cite This: J. Chem. Inf. Model. 2023, 63, 3534−3543 Read Online

ACCESS | Metrics & More | Article Recommendations | Supporting Information

ABSTRACT: The cardiac thin filament comprises F-actin, tropomyosin, and troponin (cTn). cTn is composed of three subunits: troponin C (cTnC), troponin I (cTnI), and troponin T (cTnT). To computationally study the effect of the thin filament on cTn activation events, we employed targeted molecular dynamics followed by umbrella sampling using a model of the thin filament to measure the thermodynamics of cTn transition events. Our simulations revealed that the thin filament causes an increase in the free energy required to open the cTnC hydrophobic patch and causes a more favorable interaction between this region and the cTnI switch peptide. Mutations to the cTn complex can lead to cardiomyopathy, a collection of diseases that present clinically with symptoms of hypertrophy or dilation of the cardiac muscle, leading to impairment of the heart's ability to function normally and ultimately myocardial infarction or heart failure. Upon introduction of cardiomyopathic mutations to R145 of cTnI, we observed a general decrease in the free energy of opening the cTnC hydrophobic patch, which is on par with previous experimental results. These mutations also exhibited a decrease in electrostatic interactions between cTnI-R145 and actin-E334. After introduction of a small molecule to the wild-type cTnI−actin interface to intentionally disrupt intersubunit contacts, we successfully observed similar thermodynamic consequences and disruptions to the same protein−protein contacts as observed with the cardiomyopathic mutations. Computational studies utilizing the cTn complex in isolation would have been unable to observe these effects, highlighting the importance of using a more physiologically relevant thin-filament model to investigate the global consequences of cardiomyopathic mutations to the cTn complex.

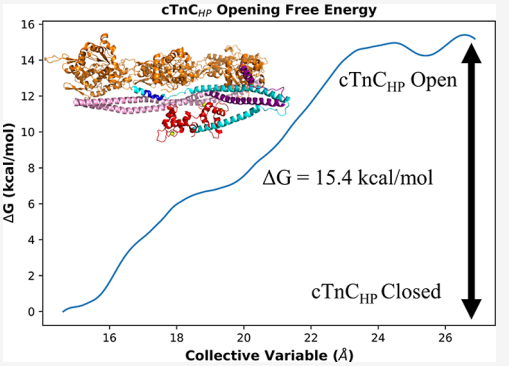

INTRODUCTION

The cardiac thin filament comprises F-actin, tropomyosin, and troponin (cTn).[1] cTn itself comprises three subunits: troponin C (cTnC) that binds Ca^{2+}, troponin I (cTnI) that has an inhibitory effect on muscle contraction, and troponin T (cTnT) that anchors the cTn complex to the thin filament.[2] During low intracellular Ca^{2+} concentration, the cTn complex is in a Ca^{2+}-unbound state, where the Ca^{2+}-binding site II of the N-terminal region of cTnC is not occupied by Ca^{2+}, and the cTnI switch peptide ($cTnI_{SP}$) and cTnI inhibitory peptide ($cTnI_{IP}$) are bound to actin. When the muscle is activated by electrical signaling from the brain, Ca^{2+} is released into the cell from the sarcoplasmic reticulum.[3] This elevation in intracellular Ca^{2+} levels causes Ca^{2+} to bind to cTnC, initiating a conformational shift in cTnC that exposes a hydrophobic patch ($cTnC_{HP}$) primed for binding the $cTnI_{SP}$, effectively removing it from its position on actin. This motion initiates the process to allow myosin heads (thick filament) to interact with actin for muscle contraction to occur.

cTnC is a dumbbell-shaped protein that contains four Ca^{2+}-binding sites in EF hand domains, labeled sites I−IV. An EF hand domain can be characterized as a helix-loop-helix motif and is the most common protein structure that binds Ca^{2+}.[4] Under physiological conditions, sites III and IV are virtually always occupied by Ca^{2+}, with site I never occupied by Ca^{2+}.[2] This leaves solely site II, a 12-residue Ca^{2+}-binding loop, to be responsible for detecting and binding Ca^{2+} when intracellular levels of the ion rise.[5] As such, it is intriguing that mutations all throughout the cTn complex (many of which are linked with cardiomyopathy) have been shown to be able to modulate Ca^{2+}-sensitivity of the myofilament.[6] Cardiomyopathy is a collection of diseases that present clinically with symptoms of hypertrophy or dilation of the cardiac muscle, leading to impairment of the heart's ability to function normally and ultimately myocardial infarction or heart failure.[7] The causes of cardiomyopathy are varied; however, most of them are genetic. Hypertrophic cardiomyopathy (HCM) and restrictive cardio-

Received: March 10, 2023
Published: June 1, 2023

myopathy (RCM) can be characterized by decreased ventricular filling, slight thickening of the heart muscle, and an increase in Ca^{2+}-sensitivity of the myofilament.[8]

For this study, we chose to investigate three mutations located in the inhibitory peptide that have been linked with cardiomyopathy: R145G, R145Q, and R145W. Experimental studies have explored the functional consequences or cause of change in Ca^{2+}-sensitivity caused by these mutations. Dvornikov et al. explored the effect of the R145W mutation on myofilament length-dependent activation (LDA) and found that the mutation does not affect LDA but does increase the sensitivity of the myofilament to Ca^{2+}.[9] Moreover, biochemical assays and functional experiments on the R145G mutation converged on the finding that this mutation causes an increase in myofilament Ca^{2+}-sensitivity[10,11] and reduces the ability of cTnI to inhibit activation of cardiac muscle.[12,13] Computational efforts have also explored the effect that these cTnI mutations can have on the thermodynamics of the $cTnC_{HP}$ opening event.[9,14−16] Our lab and others have successfully shown the potential of computational tools as a viable option for studying cTn dynamics for the purpose of computationally aided drug discovery[17−25] and Ca^{2+}-binding simulations.[26−36]

In 2011, in the absence of a structure of cTn in the context of the thin filament, the Schwartz group developed a model of the thin filament.[37] Their successive molecular dynamics (MD) simulations utilizing this model were able to elucidate functional mechanisms for the cTn complex and potential causes of disease for cTnT mutations.[38,39] Recently, using cryogenic electron microscopy (cryo-EM), Yamada and colleagues resolved the structure of the cTn complex in the context of the thin filament for the first time in both the Ca^{2+}-bound and Ca^{2+}-unbound states.[40] These structures have enabled computational studies to further understand the dynamics and function of cTn within the thin filament, a more physiologically relevant context than simulated isolated cTn.[41] We have previously studied the thermodynamics of the cTn complex in isolation using a combination of targeted MD (TMD) and umbrella sampling (US)[15] and were able to produce results that correlated with experimental[42] and computational[43] studies. However, these simulations were unable to explore the effect that actin would have on both the $cTnI_{SP}$-binding and $cTnC_{HP}$-opening events. In the Ca^{2+}-unbound state, the inhibitory and switch peptide regions of cTnI are interacting with actin in some capacity. Additionally, a few residues in helix C of the N-terminal cTnC are interacting with tropomyosin. In the Ca^{2+}-bound state, parts of the $cTnI_{IP}$ are still interacting with actin and cTnC has shifted to introduce more interactions between helices B and C with tropomyosin. Therefore, we expect the presence of actin and tropomyosin to influence the thermodynamics of the $cTnC_{HP}$ opening and $cTnI_{SP}$ binding. Utilizing a more physiologically relevant thin-filament system for simulations will allow us to make predictions more confidently about thermodynamic consequences of cardiomyopathic mutations within cardiac muscles.

In this study, we used a simplified system of the thin filament to evaluate the impact of thin-filament elements on the thermodynamics of the transition between a Ca^{2+}-unbound and Ca^{2+}-bound cTn complex. Our US simulations revealed that the thin filament causes an increase in the free energy required to open the $cTnC_{HP}$ and causes a more favorable interaction between the $cTnC_{HP}$ and the $cTnI_{SP}$. Upon introduction of cardiomyopathic mutations to R145 of cTnI, we observed a general decrease in free energy of opening the $cTnC_{HP}$, which is on par with previous experimental results. These mutations also exhibited varying effects on $cTnI_{SP}$ binding, but all caused a decrease in electrostatic interactions between cTnI-R145 and actin-E334. After introduction of a small molecule to the cTnI−actin interface, we observed similar thermodynamic consequences as seen for the cardiomyopathic mutations since the small molecule was designed to cause disruptions to the same protein−protein contacts.

Including components of actin and tropomyosin for these studies offered two advantages over previous simulations. First, the effective concentration of $cTnI_{SP}$ to the $cTnC_{HP}$ regions was increased due to the presence of actin. This created a more direct transition of the $cTnI_{SP}$ from its position in the Ca^{2+}-unbound to the Ca^{2+}-bound state. This in turn produced a TMD trajectory that would be more representative of the physiological transition, allowing us to extract windows more accurately modeling the transition states. Second, we were able to directly quantify the effect actin has on the thermodynamics of $cTnC_{HP}$ opening and $cTnI_{SP}$ binding. These results shed light on crucial cTn−actin interactions for normal function of the heart. Overall, this study highlights the viability of using computational tools in further understanding the thermodynamics of cardiac contractility.

METHODS

Model Generation. Structures of troponin, actin, and tropomyosin in both the Ca^{2+}-bound and Ca^{2+}-unbound states were necessary to simulate the transition between the two states using TMD. Instead of using a model of the thin filament that contained actin, troponin, and tropomyosin in a 7:1:1 stoichiometry, we chose to simplify the system to expedite our simulations. We extracted cTnC (chain c; residues 2−161), cTnI (chain b; residues 41−166), cTnT (chain a; residues 199−272), two subunits of tropomyosin (chains P and Q; residues 100−220 each), and 3 subunits of actin (chains E, G, and I; residues 1−375 each). Our starting model representing the Ca^{2+}-unbound state extracted these residues from PDB 6KN7, and our starting model representing the Ca^{2+}-bound state extracted these residues from PDB 6KN8 (Figure 1). The two chains of tropomyosin composed a single tropomyosin strand, and the three troponin subunits composed a single complete cTn complex. Thus, we simulated a thin-filament model in a 3:1:1 stoichiometry instead of the 7:1:1 stoichiometry in the cryo-EM structures. This was a sufficient ratio for the purpose of our simulations as the cTn complex was only in contact with three actin subunits (chains E, G, and I) in both PDB structures. We then added Ca^{2+} ions to sites II, III, and IV of cTnC in both models using Autodock Vina.[44] Although the model created from PDB 6KN7 represented a Ca^{2+}-unbound (with respect to site II) model, Ca^{2+} was docked in cTnC site II since inclusion was necessary to accurately represent the beginning model of the transition event.

TMD and Window Selection. TMD is an enhanced sampling method that steers a starting structure toward a target structure by applying an additional potential energy term, U_{TMD}, described below

$$U_{TMD} = \frac{1}{2}\frac{k}{N}[\mathrm{RMSD}(t) - \mathrm{RMSD}^*(t)]^2$$

https://doi.org/10.1021/acs.jcim.3c00388
J. Chem. Inf. Model. 2023, 63, 3534−3543

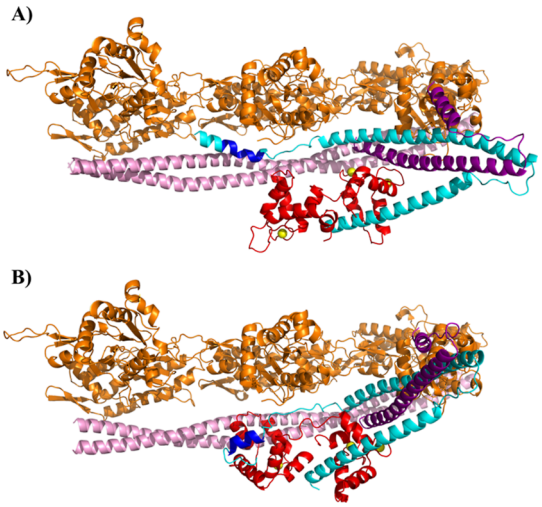

Figure 1. Cartoon representation of thin filament simulation systems. (A) Starting model for TMD simulations representing the initial state of a Ca^{2+}-unbound model before the TMD transition. The $cTnI_{SP}$–$cTnC_{HP}$ distance is 26.5 Å, and the $cTnC_{HP}$ interhelical distance is 15.7 Å. (B) Target model for TMD simulations representing the final state of the Ca^{2+}-bound thin filament. The $cTnI_{SP}$–$cTnC_{HP}$ distance is 9.5 Å, and the $cTnC_{HP}$ interhelical distance is 25.1 Å. For both models, actin is depicted in orange, tropomyosin in pink, cTnT in purple, cTnI in cyan, cTnC in red, and Ca^{2+} ions in yellow. $cTnI_{SP}$ residues 151–159 are highlighted in a dark blue. Although Figure 1A represents a Ca^{2+}-unbound model, Ca^{2+} is shown in cTnC site II due to its inclusion being necessary to model the transition to a Ca^{2+}-bound state.

where k is a force constant, and N is the number of atoms in the protein. RMSD(t) is the instantaneous best-fit root mean square distance of the current coordinates from the target coordinates at time t, and RMSD*(t) evolves linearly from the initial RMSD at the first TMD step to the final RMSD at the last TMD step. Using this method allowed us to produce a trajectory between the Ca^{2+}-unbound and Ca^{2+}-bound forms of the thin filament as observed by cryo-EM.

The TMD simulations were prepared using the same steps as described in the previous work by our group.[15] All preparation and subsequent TMD simulations were performed using NAMD 2.13 with the Charmm36 force field. The simulations were conducted under an *NPT* ensemble at 310 K with Langevin temperature and pressure dampening, using a 2 femtosecond timestep. All bonds involving hydrogens were constrained using the ShakeH algorithm, with structures being saved every 2 picoseconds. Three independent TMD simulations were performed for 60 ns to guide the Ca^{2+}-unbound starting model toward the Ca^{2+}-bound model. All non-hydrogen atoms in the troponin and tropomyosin subunits were biased toward the target structure by applying a spring constant of k = 200 kcal/mol/Å to the TMD gradient of potential energy function.

For each of the simulations, the values of the $cTnC_{HP}$ interhelical distance and $cTnI_{SP}$–$cTnC_{HP}$ distance were determined for each of the frames in the trajectory. The $cTnC_{HP}$ interhelical distance was defined as the distance between the average position of the N, C, and CA atoms of cTnC residues 14 and 48. The $cTnI_{SP}$–$cTnC_{HP}$ distance was defined as the distance between the average position of the CA atoms in $cTnC_{HP}$ residues (20, 23, 24, 26, 27, 36, 41, 44, 48, 57, 60, 77, 80, 81)[45] and the average position of the CA atoms in $cTnI_{SP}$ residues 151–159. This range of residues was selected to represent the $cTnI_{SP}$ as they are the residues that comprise the α helical region of the $cTnI_{SP}$ bound to an open $cTnC_{HP}$ in the PDB 6KN8 structure. The trial that exhibited sampling with the strongest correlation between the $cTnC_{HP}$ opening and $cTnI_{SP}$ binding events was selected as the representative trajectory.

Umbrella Sampling. US is a technique to facilitate the sampling of different protein states along a collective variable. By restraining starting models to a given value of the collective variable, the free energy of the transition between states can be evaluated based on the sampling around the defined restrained variable. From the representative TMD trajectory, 24 frames were extracted as windows to be used in US simulations. The $cTnC_{HP}$ interhelical distance of the windows ranged from 15.0 Å in window 1 to 26.4 Å in window 24. The $cTnI_{SP}$–$cTnC_{HP}$ distance of the windows ranged from 17.4 Å in window 1 to 9.3 Å in window 24. Values for the $cTnC_{HP}$ interhelical distance and $cTnI_{SP}$–$cTnC_{HP}$ distance for each window can be seen in Table S1. Each of the windows was used for two separate, independent US simulations: (1) with the collective variable defined as the $cTnC_{HP}$ interhelical distance and (2) with the collective variable defined as the $cTnC_{HP}$–$cTnI_{SP}$ distance. This allowed us to measure the free energy of each of the events ($cTnC_{HP}$ opening, $cTnI_{SP}$ binding) separately, using the same starting models. For each window, an extra harmonic restraint was applied with a force constant of 5 kcal/mol, with the center of the restraint being the collective variable listed in Table S1. The collective variables for US simulations were defined the same as previously described in TMD and Window Selection. US for each of the windows was run in triplicate, for each collective variable separately, for 50 ns at 310 K under an *NPT* ensemble and a 1 fs timestep. For US simulations of the HCM and RCM mutant systems, the Mutagenesis Wizard function, available in PyMOL,[46] was used to apply the R145G, R145Q, and R145W mutations to each of the 24 windows described above. Windows with these mutations were simulated (using US) under the same conditions as the wild-type system.

Small-Molecule Docking. To identify potential binding sites for small molecules in the cTnI–actin interface, we submitted PDB structures 6KN7 and 6KN7 to the web server FTMap.[47] This revealed a potential binding site between the inhibitory peptide region of cTnI (residues 137–148), actin residues 24–27, and actin residues 333–341. We then docked 4800 structurally diverse compounds available from the Life Chemicals General Fragment Library[48] into the Ca^{2+}-unbound thin-filament model described in *Model Generation*. Schrodinger's Maestro suite was used to prepare the ligands within a pH range of 7.4 ± 1.0 using Ligprep[49] and to generate a receptor grid using Receptor Grid Generation.[50] The center of the docking box was designated as the C-alpha atom of actin 334 in chain G, with an inner box size of 10 Å × 10 Å x 10 Å and an outer box size of 20 Å × 20 Å x 20 Å. The 6227 small molecules generated from LigPrep were docked into the receptor using GlideSP. The small molecules were ranked based on their docking scores, with the highest ranking molecule interacting with both cTnI and actin selected as the molecule used to perform US simulations on. The selected molecule, F2173-0939, was then docked into each of the 24 wild-type windows extracted for US using the same methods described above. F2173-0939 was parameterized for MD using the online server CGenFF.[51] US simulations including the

https://doi.org/10.1021/acs.jcim.3c00388
J. Chem. Inf. Model. 2023, 63, 3534–3543

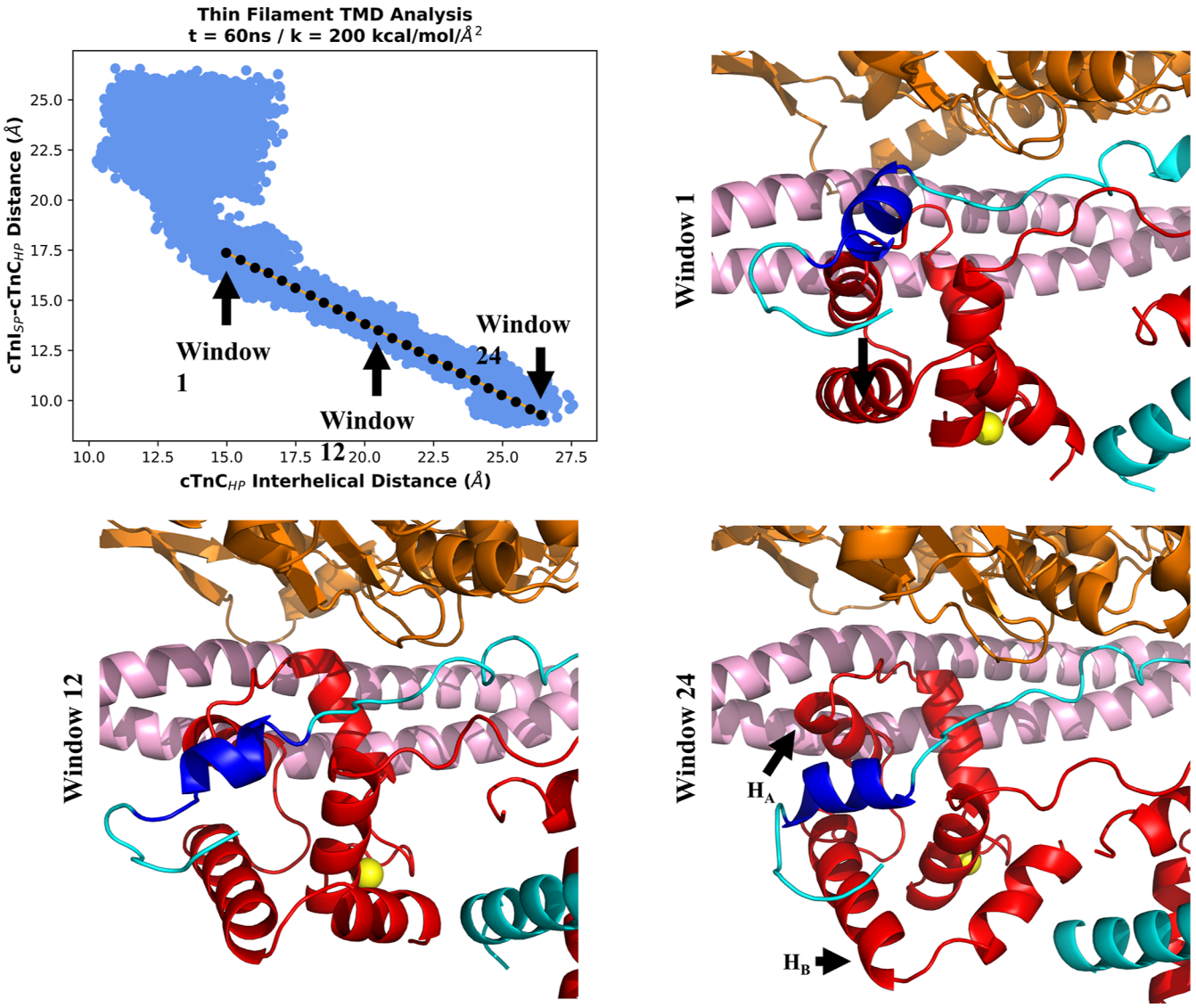

Figure 2. TMD trajectory analysis and window selection. Each point in the graph represents a frame from the TMD trajectory with the strongest correlation between the $cTnC_{HP}$ opening and $cTnI_{SP}$ binding events, located at its calculated $cTnC_{HP}$ interhelical distance and $cTnI_{SP}$–$cTnC_{HP}$ distance. A line of regression was created using all points with a $cTnI_{SP}$–$cTnC_{HP}$ distance ≤19 Å. Extracted windows for US along the line of regression are showcased using black dots with windows 1, 12, and 24 highlighted. Window 1 was centered at a $cTnI_{SP}$–$cTnC_{HP}$ distance of 17.367 Å and a cTnC interhelical distance of 14.974 Å. Window 12 was centered at a $cTnI_{SP}$–$cTnC_{HP}$ distance of 13.811 Å and a cTnC interhelical distance of 20.497 Å. Window 24 was centered at a $cTnI_{SP}$–$cTnC_{HP}$ distance of 9.280 Å and a cTnC interhelical distance of 26.407 Å. Actin is depicted in orange, tropomyosin in pink, cTnI in cyan, cTnC in red, and Ca^{2+} ion in yellow. $cTnI_{SP}$ residues 151–159 are highlighted in a dark blue. Helices A and B (residues 14–48, $cTnC_{HP}$) of cTnC are labeled H_A and H_B, respectively, in window 24.

ligand-bound systems were then performed in the exact same manner as previously described.

WHAM Free-Energy Estimation and Contact Analysis. After completion of the US simulations, we categorized the first 25 ns of each simulation as an equilibration period for the window. The collective variable applied to the window was then evaluated for each frame in the trajectory during the remaining 25 ns, producing 25 000 data points per simulation. The data for each window was combined across the three independent simulations, producing 75 000 data points per window and 1.8 million data points per collective variable. Free energies were computed from this data for each collective variable and each system using the weighted histogram analysis method (WHAM) by Alan Grossfield.[52] The minimum and maximum values used for the $cTnC_{HP}$ interhelical distance were set as 14.5 and 27.0 Å, with the minimum and maximum values of the $cTnI_{SP}$–$cTnC_{HP}$ distance set as 8.0 and 17.8 Å. The histogram analysis for both collective variables was divided into 50 bins, using a tolerance of 10^{-6}, and a force constant of 10 kcal/mol. The adjustment of the force constant is necessary as the charmm36 force field does not include a 1/2 in the force constant restraint terms, yet the code for WHAM does. This necessary adjustment is described in "An implementation of WHAM: the Weighted Histogram Analysis Method" by Alan Grossfield.[52] This method of producing free-energy profiles for both collective variables was applied to all systems discussed: wild-type, R145G, R145Q, R145W, and the F2173-0939 ligand bound systems.

https://doi.org/10.1021/acs.jcim.3c00388
J. Chem. Inf. Model. 2023, 63, 3534–3543

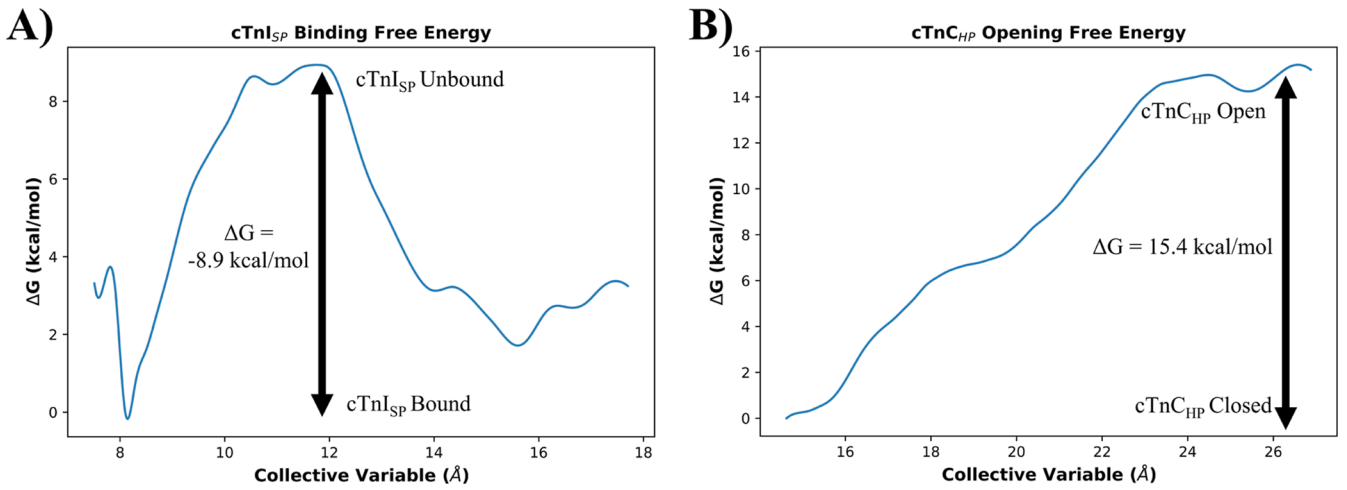

Figure 3. Free-energy curves for $cTnI_{SP}$ binding and $cTnC_{HP}$ opening in the wild-type system. (A) Free energy across the $cTnI_{SP}$−$cTnC_{HP}$ binding event for the wild-type system. Binding occurs right (12 Å) to left (8 Å) as the distance between the two entities decreases. (B) Free energy across the $cTnC_{HP}$ opening event for the wild-type system. The $cTnC_{HP}$ opens from left (15 Å) to right (26.5 Å).

RESULTS

TMD Simulations Sample Conformational Changes of Thin Filament upon Ca^{2+} Binding, $cTnC_{HP}$ Opening, and $cTnI_{SP}$ Binding. TMD simulations were used to obtain a trajectory of the transition between the Ca^{2+}-unbound and Ca^{2+}-bound structures of the thin filament. We ran three independent simulations for 60 ns using a force constant of 200 kcal/mol/Å^2. This simulation time and force constant were shown to be optimal for observing a smooth transition within the cTn complex in our previous work.[15] For each of the 30 000 frames produced by each of the three trajectories, the $cTnC_{HP}$ interhelical distance and the $cTnI_{SP}$−$cTnC_{HP}$ distance were evaluated. We were able to observe a gradual transition from a $cTnI_{SP}$-unbound, closed $cTnC_{HP}$ model to a $cTnI_{SP}$-bound, open $cTnC_{HP}$ model. Using all simulation data points that exhibited a $cTnI_{SP}$−$cTnC_{HP}$ distance ≤19 Å, we created a line of regression for each of the trials. This allowed us to characterize how the $cTnC_{HP}$ opening and $cTnI_{SP}$ binding events correlated with each other. Data used to create the line of regression included simulation frames with a $cTnC_{HP}$ interhelical distance between 12.4 and 27.6 Å and $cTnI_{SP}$−$cTnC_{HP}$ distances between 8.9 and 19.0 Å. The trajectory that had the strongest correlation between $cTnC_{HP}$ opening and $cTnI_{SP}$ binding events was selected to extract frames for US simulations. Figure 2 shows these results for the representative TMD trajectory, and the trajectory can be viewed in Video S1.

To obtain US windows that would cover the entire reaction coordinate of the $cTnC_{HP}$ opening event, we set target distances between 15 and 26.5 Å of every 0.5 Å. Using the equation for the line of regression, we were then able to extract windows with data closest to the target values of both collective variables. Doing this allowed us to obtain thin-filament models with a $cTnI_{SP}$−$cTnC_{HP}$ distance ranging between 9 and 17.5 Å. This process produced a total of 24 windows that contained models along the transition starting at a $cTnI_{SP}$-unbound, closed $cTnC_{HP}$ (window 1: $cTnC_{HP}$ interhelical distance = 15 Å, $cTnI_{SP}$−$cTnC_{HP}$ distance = 17.4 Å) and ending with a model representing a $cTnI_{SP}$-bound, open $cTnC_{HP}$ (window 24: $cTnC_{HP}$ interhelical distance = 26.4 Å, $cTnI_{SP}$−$cTnC_{HP}$ distance = 9.2 Å). Figure 2 shows the starting model used in US for windows 1, 12, and 24 from this selection process.

US Reveals the Effect of Thin Filament on Troponin Thermodynamics. We performed independent 50 ns US simulations for each of the two collective variables for each of the 24 windows in triplicate. Due to the complexity of the thin-filament system being simulated, we categorized the first 25 ns of each simulation as equilibration time and only utilized data from the final 25 ns to estimate free energies, similar to the strategy described in Domański et al.[53] For each simulation trajectory, the collective variable applied ($cTnC_{HP}$ interhelical distance or $cTnI_{SP}$−$cTnC_{HP}$ distance, respectively) was evaluated for each of the frames in the final 25 ns, and the data across the three trials was combined as described in Methods. This allowed us to obtain 75 000 data points per window and to evaluate 1.8 million data points per collective variable. Analysis of the data showed sufficient overlap between neighboring windows (Figure S1), indicating that we were able to sample the entire reaction coordinate. Using WHAM,[52] we evaluated the free energy of the $cTnC_{HP}$ opening event to be 15.4 ± 0.2 kcal/mol and the $cTnI_{SP}$−$cTnC_{HP}$ binding free energy to be −8.9 ± 0.1 kcal/mol. The free-energy curves created from this analysis are shown in Figure 3. Evaluation of the free-energy convergence revealed that a simulation time of 25 ns was sufficient to reach convergence for both collective variables (Figure S2). The free energy of the $cTnC_{HP}$ opening only changed by less than 0.5 kcal/mol over the last 10 ns, and the free energy of $cTnI_{SP}$ binding only changed by less than 0.2 kcal/mol over the last 15 ns. We evaluated error for the reported free-energy values by determining the standard deviation of free-energy values determined by WHAM every 0.1 ns over the final 15 ns of the US simulations.

We had previously estimated the free energy of opening the $cTnC_{HP}$ in the absence of actin and tropomyosin, using virtually the same TMD/US protocol described here, as 12.0 kcal/mol.[15] We therefore estimate that the thin filament increases the free energy required to open the patch by about 3.4 kcal/mol. Experimental studies have shown that the addition of actin and tropomyosin decreases Ca^{2+}-sensitivity to cTnC[54] and that increases in Ca^{2+}-sensitivity allow the $cTnC_{HP}$ to be able to be opened easier.[55] Therefore, the observed trend of increased free energy of opening the $cTnC_{HP}$ upon addition

https://doi.org/10.1021/acs.jcim.3c00388
J. Chem. Inf. Model. 2023, 63, 3534−3543

of the thin-filament components agrees with the experimental results as a more complex system decreases Ca^{2+}-sensitivity, which could plausibly be facilitated by an increase in free energy required to open the $cTnC_{HP}$.

Using 2D (^1H,^{15}N) HSQC NMR spectroscopy, the $cTnI_{SP}$ binding affinity (K_D) to N-terminal cTnC had been measured at 154 μM (corresponding to a ΔG of −5.2 kcal/mol),[56] which we were able to accurately replicate in previous simulations of the isolated cTn complex.[15] To our knowledge, $cTnI_{SP}$ binding affinity to $cTnC_{HP}$ has not been directly measured within the thin-filament system simulated here; however, Robertson et al. have shown that increasing the complexity of the components involved in this binding event increased the affinity of the $cTnI_{SP}$ to the $cTnC_{HP}$ (ΔG of −6.3 kcal/mol).[57] Our results would support their findings as we saw a significant increase in binding affinity from our previous cTn complex simulations (−5.4 kcal/mol) to our current results that estimate the binding affinity at −8.9 kcal/mol. This observation may highlight the importance of actin and tropomyosin in promoting the interaction between cTnI and cTnC during muscle contraction.

Mutations to R145 Generally Cause a Decrease in Free Energy of Opening Hydrophobic Patch. For all 24 windows, we applied the R145G, R145Q, and R145W cardiomyopathic mutations to cTnI using the Mutagenesis Wizard function available in PyMOL.[46] We then subjected the 24 windows to US simulations to measure the $cTnC_{HP}$ opening and $cTnI_{SP}$ binding free energies using the same process described above. Subsequent WHAM analysis of the US simulations allowed us to determine the effect of the mutations of the free energies of these events in the context of the thin filament (Table 1).

Table 1. Free Energies of $cTnC_{HP}$ Opening and $cTnI_{SP}$ Binding[a]

model	disease	ΔG $cTnC_{HP}$ opening (kcal/mol)	ΔG $cTnI_{SP}$ binding (kcal/mol)
wild-type		15.4 ± 0.2	−8.9 ± 0.1
R145G	HCM	13.9 ± 0.2	−11.5 ± 0.2
R145Q	RCM	14.9 ± 0.7	−7.8 ± 0.2
R145W	RCM	14.9 ± 0.1	−5.5 ± 0.5

[a]Data shown for wild-type, HCM, and RCM systems.

Biochemical assays and activity experiments on R145G and R145W have shown that these mutations increase Ca^{2+}-sensitivity of cTn when in the context of the thin filament.[10,11,58] We have previously hypothesized and shown in computational studies that R145G increased the propensity of the $cTnC_{HP}$ to be in the open state,[14] effectively lowering the free energy of opening the $cTnC_{HP}$.[43] We again here show that both the HCM mutation R145G and the RCM mutations R145Q and R145W lower the free energy of opening the $cTnC_{HP}$. We observed a more significant decrease in the $cTnC_{HP}$ opening ΔG for the R145G system ($\Delta\Delta G$ = −1.5 kcal/mol) when compared to both RCM mutations ($\Delta\Delta G$ = −0.5 kcal/mol).

Mutations to R145 Exhibit Varied Effects on Switch Peptide Binding Free Energy. Evaluation of the free energy of the $cTnI_{SP}$ binding to the $cTnC_{HP}$ in the presence of cardiomyopathic mutations revealed that R145G promoted binding ($\Delta\Delta G$ = −2.6 kcal/mol), while the R145Q and R145W systems reduced the binding affinity ($\Delta\Delta G$ = +1.1 kcal/mol and +3.4 kcal/mol, respectively). As we are unaware of any experimental research that has directly measured the binding affinity of the $cTnI_{SP}$ to the $cTnC_{HP}$ of a mutant cTn complex in the context of the thin filament, we were unable to compare these values to previous studies. In order to elucidate a potential cause of these thermodynamic shifts upon introduction of cardiomyopathic mutations, we performed contact analysis of cTnI-145 to residues in the actin subunit most closely associated with cTnI. We designated a contact as a residue in actin with a C-beta atom (C-alpha atom for glycine) within 8 Å of the C-beta atom of cTnI-145. For each system, the ratio of contact time was determined throughout all triplicate $cTnI_{SP}$−$cTnC_{HP}$ collective variable window simulations and compared between the mutant and wild-type systems. From this analysis, two significant observations were made: (1) all three mutations caused a decrease in contact between cTnI-145 and actin-334 by at least 28.4% and (2) all three mutations caused an increase in contact between cTnI-145 and actin-348 by at least 32.2% (Table 2).

Table 2. Analysis of cTnI-145 Contact with Actin Residues[a]

model	disease	actin-E334	actin-S348
wild-type		34.1% ± 3.1%	46.0% ± 6.4%
R145G	HCM	2.0% ± 1.2%	63.9% ± 8.7%
R145Q	RCM	24.4% ± 5.0%	60.8% ± 1.6%
R145W	RCM	10.2% ± 3.2%	63.0% ± 4.6%

[a]Total percentage of simulation time that cTnI-R145 was in contact with residues actin-E334 and actin-S348. Values reflect data across all frames in the US window simulations that evaluated the $cTnI_{SP}$−$cTnC_{HP}$ collective variable.

In the wild-type system, we observed notable charge−charge interactions between the positively charged cTnI-145 arginine residue and the negatively charged glutamate in actin-334. Upon introduction of the mutations to glycine, glutamine, or tryptophan, this attractive charge−charge interaction was significantly disrupted. In general, electrostatic interactions in protein−protein complexes have been shown to be highly important in their structural and thermodynamic stability.[59] Our results suggest that these mutations potentially destabilized the cTn−actin interface, leading to differences in measured $cTnI_{SP}$ binding free energies. The observed increased interactions of the restrictive cardiomyopathic mutation residues to actin-348 (serine) may have been caused by an increase in hydrogen bond interactions between cTnI-145 and actin-348. The R145G mutation may have experienced a decrease in interactions with actin-334 due to the relatively small glycine side chain not being able to reach the actin-334 residue. The glycine residue would then have had a higher probability of interacting with actin-348 due to its closer starting position to cTnI-145 than actin-334.

Small Molecule in cTnI−Actin Interface Mimics RCM Thermodynamic Effects. To further test the idea of destabilization in the cTnI−actin interface as a cause for thermodynamic consequences in mutant cTn function, we intentionally introduced a small molecule to the protein−protein interface to disrupt the intersubunit contacts. We submitted our Ca^{2+}-unbound and Ca^{2+}-bound wild-type thin-filament models to the FTMap server for identification of potential small-molecule binding sites. For both models, the server identified a site in the space between the cTnI inhibitory peptide and F-actin (Figure 4A). Using this knowledge, we

https://doi.org/10.1021/acs.jcim.3c00388
J. Chem. Inf. Model. 2023, 63, 3534−3543

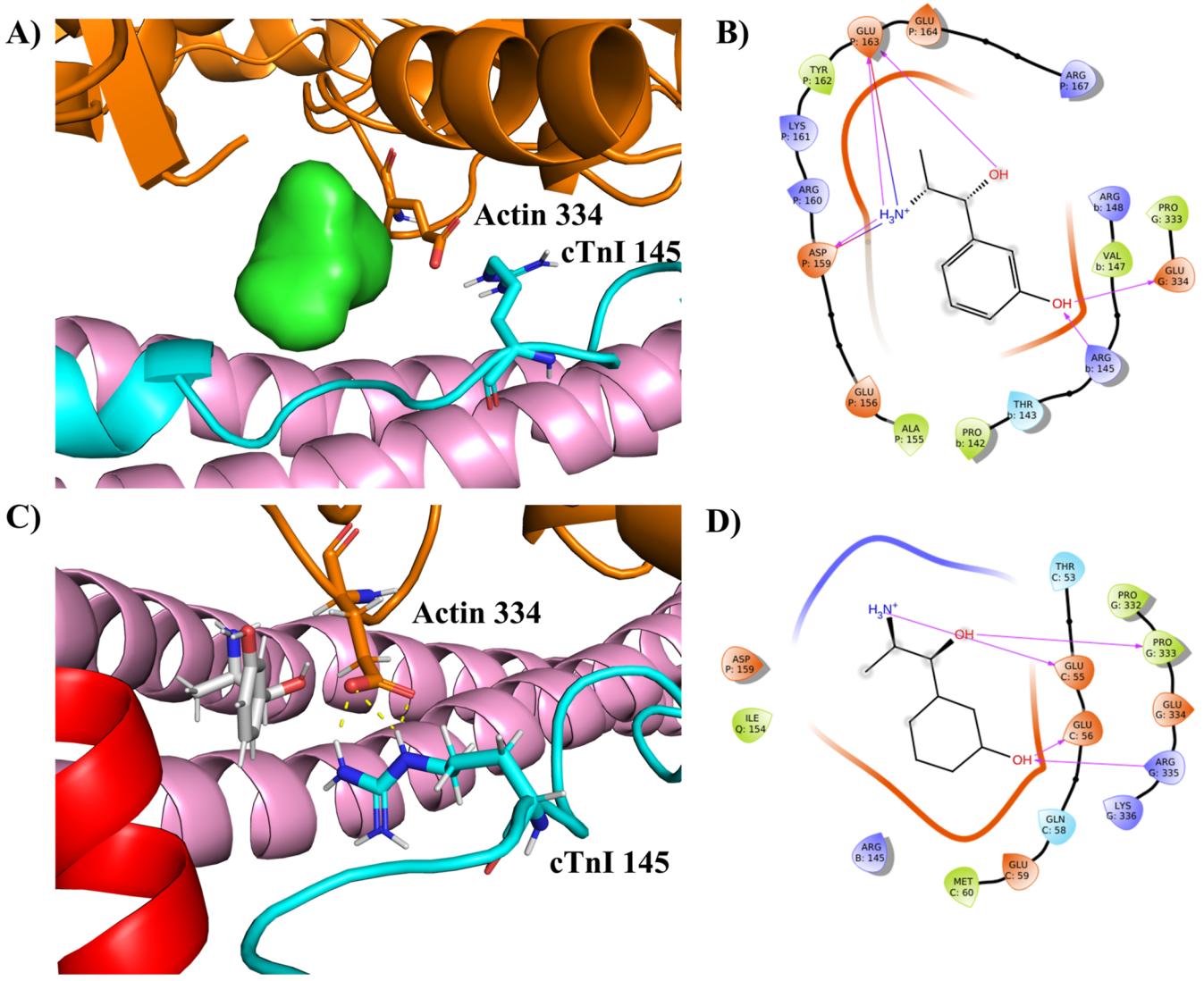

Figure 4. Small-molecule docking studies. (A) Results from FTMap binding site prediction of Ca^{2+}-unbound thin-filament system used in TMD and US. The potential binding site is shown in green, actin in orange, cTnI in cyan, and tropomyosin in pink. Residues actin 334 and cTnI 145 are shown in stick representation. (B) Ligand interaction diagram of small-molecule fragment F2173-0939 interacting with the Ca^{2+}-unbound thin-filament wild-type model. Fragment is shown in molecular structure representation, with residues in colored spheres. Chain G refers to actin, chain P refers to tropomyosin, and chain B refers to cTnI. Hydrogen bond interactions are displayed with arrows. (C) Fragment F2173-0939 docked into US window 24. Fragment is represented in gray, cTnC in red, with the rest of the image represented exactly as Figure 4A. Electrostatic interactions between Actin 334 and cTnI 145 are shown in dotted yellow lines. (D) Ligand interaction diagram of the small-molecule fragment F2173-0939 interacting with window 24 of US simulations. Figure displayed the same as panel B.

performed a docking simulation of the 4800 unique molecules contained in the Life Chemicals General Fragment Library.[48] These molecules were docked into our Ca^{2+}-unbound thin-filament system with actin-E334 as the center for the docking using Maestro's GlideSP. After ranking the results by docking score, we checked the docked positions of the top scoring molecules and found that the third highest ranked molecule, F2173-0939, had the most favorable docking score of any compound that was interacting with both cTnI and actin (Figure 4B, Table S2).

This molecule was then docked into each of the 24 wild-type starting model windows (Figure 4C,D), again using actin-E334 as the center for docking. Subsequently, we performed 50 ns US simulations on these ligand-bound systems. The results were analyzed exactly as before for the wild-type and cardiomyopathic mutation systems, producing a free energy of opening the $cTnC_{HP}$ of 13.8 ± 0.5 kcal/mol and a $cTnI_{SP}$ binding free energy of −8.1 ± 0.1 kcal/mol. These values show the same $cTnC_{HP}$ opening trend that we observed for all cardiomyopathic mutations and the same $cTnI_{SP}$ binding trend that we observed for the RCM mutations when compared to WT. Contact analysis of cTnI-R145 to actin residues revealed that F2173-0939 caused either a significant decrease in most contacts or otherwise no change. $cTnI_{SP}$ contact with actin-E334 was reduced from 34.1 to 22.4% and contact with actin-S348 was reduced from 46.0 to 34.3%. As we hypothesized, the small molecule introduced to the protein−protein interface reduced contacts of cTnI-R145 to actin residues, leading to the same thermodynamic consequences as the RCM mutations.

CONCLUSIONS

We used a simplified system of the thin filament to evaluate the impact of thin-filament elements on the thermodynamics of

https://doi.org/10.1021/acs.jcim.3c00388
J. Chem. Inf. Model. 2023, 63, 3534−3543

the transition between a Ca^{2+}-unbound and Ca^{2+}-bound cTn complex. Our US simulations revealed that the thin filament causes an increase in the free energy required to open the $cTnC_{HP}$ and causes a more favorable interaction between the $cTnC_{HP}$ and the $cTnI_{SP}$. Upon introduction of cardiomyopathic mutations to R145 of cTnI, we observed a general decrease in free energy of opening the $cTnC_{HP}$, which is on par with previous experimental results. These mutations also exhibited varying effects on $cTnI_{SP}$ binding but all caused a decrease in electrostatic interactions between cTnI-R145 and actin-E334. After introduction of a small molecule to the cTnI−actin interface to intentionally disrupt cTnI−actin intersubunit contacts, we successfully observed similar thermodynamic consequences as seen for the cardiomyopathic mutations and disruptions to the same protein−protein contacts.

This leads us to propose that interactions between cTnI and actin could be the focus of future drug discovery efforts where small molecules could be introduced to the subunit interface to promote the interaction of cTnI and actin to reverse effects of disease caused by cardiomyopathic mutations to this region. Our computational docking process could be employed in a reverse fashion to identify potential small molecules that increase interactions. Additionally, it is important to highlight that previous computational studies utilizing only the isolated cTn complex were unable to observe the increase in free energy of $cTnC_{HP}$ opening and more favorable $cTnI_{SP}$ binding that was measured in the presence of actin and tropomyosin. This underscores the importance of using a more physiologically relevant thin-filament model to study global consequences of cardiomyopathic mutations.

■ ASSOCIATED CONTENT

Data Availability Statement

The wild-type cTn protein structures (6KN7, 6KN8) were available in the Protein Data Bank (PDB) at https://www.rcsb.org/. All mutations were created using the wild-type protein structure as the base model within the PyMOL software using the protein mutagenesis tool. All TMD and US simulations were performed within the NAMD Version 2.13 framework. Weighted Histogram Analysis Method (WHAM) was performed using WHAM Version 2.0.11 available at http://membrane.urmc.rochester.edu/?page_id=126. The Life Chemicals General Fragment Library is available at https://lifechemicals.com/fragment-libraries/general-fragment-library. Maestro's Ligprep, Receptor Grid Generation, and Glide SP functionalities were used for all docking simulations.[60] Additionally, we have produced a zip file of all input scripts and models necessary to perform the TMD simulations on the WT model of the thin filament, and US simulations of the WT, R145G, R145Q, R145W, and F2173-0939 docked models. These files can be found at: https://doi.org/10.5061/dryad.rv15dv4cr.

Supporting Information

The Supporting Information is available free of charge at https://pubs.acs.org/doi/10.1021/acs.jcim.3c00388.

Values for the collective variables for each of the windows used in US, coverage of collective variables during umbrella sampling simulations, convergence of WHAM estimated free energy during umbrella sampling simulations, and top 30 scoring fragments from docking study (PDF)

Representative TMD trajectory (MP4)

■ AUTHOR INFORMATION

Corresponding Author

Steffen Lindert − *Department of Chemistry and Biochemistry, The Ohio State University, Columbus, Ohio 43210, United States*; orcid.org/0000-0002-3976-3473; Phone: 614-292-8284; Email: lindert.1@osu.edu; Fax: 614-292-1685

Author

Austin M. Cool − *Department of Chemistry and Biochemistry, The Ohio State University, Columbus, Ohio 43210, United States*

Complete contact information is available at: https://pubs.acs.org/10.1021/acs.jcim.3c00388

Notes

The authors declare no competing financial interest.

■ ACKNOWLEDGMENTS

The authors would like to thank members of the Lindert Lab for their discussions and suggestions as well as the Ohio Supercomputer Center[61] for valuable computational resources. This work was supported by the NIH (R01 HL137015 to S.L.).

■ REFERENCES

(1) Risi, C. M.; Pepper, I.; Belknap, B.; Landim-Vieira, M.; White, H. D.; Dryden, K.; Pinto, J. R.; Chase, P. B.; Galkin, V. E. The structure of the native cardiac thin filament at systolic Ca2+ levels. *Proc. Natl. Acad. Sci. U.S.A.* **2021**, *118*, No. e2024288118.

(2) Marston, S.; Zamora, J. E. Troponin structure and function: a view of recent progress. *J. Muscle Res. Cell Motil.* **2019**, *41*, 71−89.

(3) Kobayashi, T.; Solaro, R. J. Calcium, thin filaments, and the integrative biology of cardiac contractility. *Annu. Rev. Physiol.* **2005**, *67*, 39−67.

(4) Lewit-Bentley, A.; Réty, S. EF-hand calcium-binding proteins. *Curr. Opin. Struct. Biol.* **2000**, *10*, 637−643.

(5) Grabarek, Z. Insights into modulation of calcium signaling by magnesium in calmodulin, troponin C and related EF-hand proteins. *Biochim. Biophys. Acta, Mol. Cell Res.* **2011**, *1813*, 913−921.

(6) Lu, Q.-W.; Wu, X. Y.; Morimoto, S. Inherited cardiomyopathies caused by troponin mutations. *J. Geriatr. Cardiol.* **2013**, *10*, 91−101.

(7) Ciarambino, T.; Menna, G.; Sansone, G.; Giordano, M. Cardiomyopathies: An Overview. *Int. J. Mol. Sci.* **2021**, *22*, 7722.

(8) Wexler, R.; Elton, T.; Pleister, A.; Feldman, D. Cardiomyopathy: an overview. *Am. Fam. Physician* **2009**, *79*, 778.

(9) Dvornikov, A. V.; Smolin, N.; Zhang, M.; Martin, J. L.; Robia, S. L.; de Tombe, P. P. Restrictive cardiomyopathy troponin I R145W mutation does not perturb myofilament length-dependent activation in human cardiac sarcomeres. *J. Biol. Chem.* **2016**, *291*, 21817−21828.

(10) Siddiqui, J. K.; Tikunova, S. B.; Walton, S. D.; Liu, B.; Meyer, M.; de Tombe, P. P.; Neilson, N.; Kekenes-Huskey, P. M.; Salhi, H. E.; Janssen, P. M.; et al. Myofilament Calcium Sensitivity: Consequences of the Effective Concentration of Troponin I. *Front. Physiol.* **2016**, *7*, 632.

(11) Deng, Y.; Schmidtmann, A.; Redlich, A.; Westerdorf, B.; Jaquet, K.; Thieleczek, R. Effects of phosphorylation and mutation R145G on human cardiac troponin I function. *Biochemistry* **2001**, *40*, 14593−14602.

(12) Lang, R.; Gomes, A. V.; Zhao, J.; Miller, T.; Potter, J. D.; Housmans, P. R. Functional analysis of a troponin I (R145G) mutation associated with familial hypertrophic cardiomyopathy. *J. Biol. Chem.* **2002**, *277*, 11670−11678.

(13) Wen, Y.; Pinto, J. R.; Gomes, A. V.; Xu, Y.; Wang, Y.; Wang, Y.; Potter, J. D.; Kerrick, W. G. L. Functional consequences of the human

cardiac troponin I hypertrophic cardiomyopathy mutation R145G in transgenic mice. *J. Biol. Chem.* **2008**, *283*, 20484−20494.
(14) Lindert, S.; Cheng, Y.; Kekenes-Huskey, P.; Regnier, M.; McCammon, J. A. Effects of HCM cTnI mutation R145G on troponin structure and modulation by PKA phosphorylation elucidated by molecular dynamics simulations. *Biophys. J.* **2015**, *108*, 395−407.
(15) Cool, A. M.; Lindert, S. Umbrella Sampling Simulations Measure Switch Peptide Binding and Hydrophobic Patch Opening Free Energies in Cardiac Troponin. *J. Chem. Inf. Model.* **2022**, *62*, 5666−5674.
(16) Cool, A. M.; Lindert, S. Computational Methods Elucidate Consequences of Mutations and Post-translational Modifications on Troponin I Effective Concentration to Troponin C. *J. Phys. Chem. B* **2021**, *125*, 7388−7396.
(17) Coldren, W. H.; Tikunova, S. B.; Davis, J. P.; Lindert, S. Discovery of Novel Small-Molecule Calcium Sensitizers for Cardiac Troponin C: A Combined Virtual and Experimental Screening Approach. *J. Chem. Inf. Model.* **2020**, *60*, 3648−3661.
(18) Aprahamian, M. L.; Tikunova, S. B.; Price, M. V.; Cuesta, A. F.; Davis, J. P.; Lindert, S. Successful Identification of Cardiac Troponin Calcium Sensitizers Using a Combination of Virtual Screening and ROC Analysis of Known Troponin C Binders. *J. Chem. Inf. Model.* **2017**, *57*, 3056−3069.
(19) Cai, F.; Li, M. X.; Pineda-Sanabria, S. E.; Gelozia, S.; Lindert, S.; West, F.; Sykes, B. D.; Hwang, P. M. Structures reveal details of small molecule binding to cardiac troponin. *J. Mol. Cell. Cardiol.* **2016**, *101*, 134−144.
(20) Lindert, S.; Li, M. X.; Sykes, B. D.; McCammon, J. A. Computer-aided drug discovery approach finds calcium sensitizer of cardiac troponin. *Chem. Biol. Drug Des.* **2015**, *85*, 99−106.
(21) Varughese, J. F.; Li, Y. Molecular dynamics and docking studies on cardiac troponin C. *J. Biomol. Struct. Dyn.* **2011**, *29*, 123−135.
(22) Varughese, J. F.; Baxley, T.; Chalovich, J. M.; Li, Y. A computational and experimental approach to investigate bepridil binding with cardiac troponin. *J. Phys. Chem. B* **2011**, *115*, 2392−2400.
(23) Pineda-Sanabria, S. E.; Julien, O.; Sykes, B. D. Versatile cardiac troponin chimera for muscle protein structural biology and drug discovery. *ACS Chem. Biol.* **2014**, *9*, 2121−2130.
(24) Hantz, E. R.; Tikunova, S. B.; Belevych, N.; Davis, J. P.; Reiser, P. J.; Lindert, S. Targeting Troponin C with Small Molecules Containing Diphenyl Moieties: Calcium Sensitivity Effects on Striated Muscle and Structure Activity Relationship. 2023. https://www.biorxiv.org/content/10.1101/2023.02.06.527323v1 (accessed May 19, 2023).
(25) Bowman, J. D.; Lindert, S. Computational Studies of Cardiac and Skeletal Troponin. *Front. Mol. Biosci.* **2019**, *6*, 68.
(26) Lindert, S.; Kekenes-Huskey, P. M.; Huber, G.; Pierce, L.; McCammon, J. A. Dynamics and calcium association to the N-terminal regulatory domain of human cardiac troponin C: a multiscale computational study. *J. Phys. Chem. B* **2012**, *116*, 8449−8459.
(27) Rayani, K.; Hantz, E. R.; Haji-Ghassemi, O.; Li, A. Y.; Spuches, A. M.; Van Petegem, F.; Solaro, R. J.; Lindert, S.; Tibbits, G. F. The effect of Mg(2+) on Ca(2+) binding to cardiac troponin C in hypertrophic cardiomyopathy associated TNNC1 variants. *FEBS J.* **2022**, *289*, 7446−7465.
(28) Rayani, K.; Seffernick, J.; Li, A. Y.; Davis, J. P.; Spuches, A. M.; Van Petegem, F.; Solaro, R. J.; Lindert, S.; Tibbits, G. F. Binding of calcium and magnesium to human cardiac troponin C. *J. Biol. Chem.* **2021**, *296*, 100350.
(29) Hantz, E. R.; Lindert, S. Adaptative Steered Molecular Dynamics Study of Mutagenesis Effects on Calcium Affinity in the Regulatory Domain of Cardiac Troponin C. *J. Chem. Inf. Model.* **2021**, *61*, 3052−3057.
(30) Hantz, E. R.; Lindert, S. Computational Exploration and Characterization of Potential Calcium Sensitizing Mutations in Cardiac Troponin C. *J. Chem. Inf. Model.* **2022**, *62*, 6201−6208.
(31) Dewan, S.; McCabe, K. J.; Regnier, M.; McCulloch, A. D.; Lindert, S. Molecular Effects of cTnC DCM Mutations on Calcium Sensitivity and Myofilament Activation-An Integrated Multiscale Modeling Study. *J. Phys. Chem. B* **2016**, *120*, 8264−8275.
(32) Lim, C. C.; Yang, H.; Yang, M.; Wang, C.-K.; Shi, J.; Berg, E. A.; Pimentel, D. R.; Gwathmey, J. K.; Hajjar, R. J.; Helmes, M.; et al. A novel mutant cardiac troponin C disrupts molecular motions critical for calcium binding affinity and cardiomyocyte contractility. *Biophys. J.* **2008**, *94*, 3577−3589.
(33) Kataoka, A.; Hemmer, C.; Chase, P. B. Computational simulation of hypertrophic cardiomyopathy mutations in Troponin I: Influence of increased myofilament calcium sensitivity on isometric force, ATPase and [Ca2+]. *J. Biomech.* **2007**, *40*, 2044−2052.
(34) Stevens, C. M.; Rayani, K.; Singh, G.; Lotfalisalmasi, B.; Tieleman, D. P.; Tibbits, G. F. Changes in the dynamics of the cardiac troponin C molecule explain the effects of Ca2+-sensitizing mutations. *J. Biol. Chem.* **2017**, *292*, 11915−11926.
(35) Skowronsky, R. A.; Schroeter, M.; Baxley, T.; Li, Y.; Chalovich, J. M.; Spuches, A. M. Thermodynamics and molecular dynamics simulations of calcium binding to the regulatory site of human cardiac troponin C: evidence for communication with the structural calcium binding sites. *JBIC, J. Biol. Inorg. Chem.* **2013**, *18*, 49−58.
(36) Kekenes-Huskey, P. M.; Lindert, S.; McCammon, J. A. Molecular basis of calcium-sensitizing and desensitizing mutations of the human cardiac troponin C regulatory domain: a multi-scale simulation study. *PLoS Comput. Biol.* **2012**, *8*, No. e1002777.
(37) Manning, E. P.; Tardiff, J. C.; Schwartz, S. D. A model of calcium activation of the cardiac thin filament. *Biochemistry* **2011**, *50*, 7405−7413.
(38) Manning, E. P.; Tardiff, J. C.; Schwartz, S. D. Molecular effects of familial hypertrophic cardiomyopathy-related mutations in the TNT1 domain of cTnT. *J. Mol. Biol.* **2012**, *421*, 54−66.
(39) Williams, M. R.; Lehman, S. J.; Tardiff, J. C.; Schwartz, S. D. Atomic resolution probe for allostery in the regulatory thin filament. *Proc. Natl. Acad. Sci. U.S.A.* **2016**, *113*, 3257−3262.
(40) Yamada, Y.; Namba, K.; Fujii, T. Cardiac muscle thin filament structures reveal calcium regulatory mechanism. *Nat. Commun.* **2020**, *11*, 153−159.
(41) Mason, A. B.; Tardiff, J. C.; Schwartz, S. D. Free-Energy Surfaces of Two Cardiac Thin Filament Conformational Changes during Muscle Contraction. *J. Phys. Chem. B* **2022**, *126*, 3844−3851.
(42) Li, M. X.; Saude, E. J.; Wang, X.; Pearlstone, J. R.; Smillie, L. B.; Sykes, B. D. Kinetic studies of calcium and cardiac troponin I peptide binding to human cardiac troponin C using NMR spectroscopy. *Eur. Biophys. J.* **2002**, *31*, 245−256.
(43) Bowman, J. D.; Lindert, S. Molecular Dynamics and Umbrella Sampling Simulations Elucidate Differences in Troponin C Isoform and Mutant Hydrophobic Patch Exposure. *J. Phys. Chem. B* **2018**, *122*, 7874−7883.
(44) Trott, O.; OlsonVina, A. J. AutoDock improving the speed and accuracy of docking with a new scoring function, efficient optimization, and multithreading. *J. Comput. Chem.* **2010**, *31*, 455−461.
(45) Wang, D.; Robertson, I. M.; Li, M. X.; McCully, M. E.; Crane, M. L.; Luo, Z.; Tu, A. Y.; Daggett, V.; Sykes, B. D.; Regnier, M. Structural and functional consequences of the cardiac troponin C L48Q Ca(2+)-sensitizing mutation. *Biochemistry* **2012**, *51*, 4473−4487.
(46) Lilkova, E.; et al. *The PyMOL Molecular Graphics System*, Version 2.0; Schrödinger, LLC, 2015.
(47) Kozakov, D.; Grove, L. E.; Hall, D. R.; Bohnuud, T.; Mottarella, S. E.; Luo, L.; Xia, B.; Beglov, D.; Vajda, S. The FTMap family of web servers for determining and characterizing ligand-binding hot spots of proteins. *Nat. Protoc.* **2015**, *10*, 733−755.
(48) Life Chemicals - General Fragment Library.
(49) Schrödinger Release 2019-1. *LigPrep*; Schrödinger, LLC: New York, NY, 2019.
(50) Schrödinger Release 2019-1. *Glide*; Schrödinger, LLC: New York, NY, 2019.

https://doi.org/10.1021/acs.jcim.3c00388
J. Chem. Inf. Model. 2023, 63, 3534−3543

(51) Vanommeslaeghe, K.; MacKerell, A. D. Automation of the CHARMM General Force Field (CGenFF) I: bond perception and atom typing. *J. Chem. Inf. Model.* **2012**, *52*, 3144−3154.
(52) Grossfield, A. WHAM: the weighted histogram analysis method, version 2.0.11, http://membrane.urmc.rochester.edu/wordpress/?page_id=126, accessed August 15th, 2022.
(53) Domański, J.; Hedger, G.; Best, R. B.; Stansfeld, P. J.; Sansom, M. S. Convergence and sampling in determining free energy landscapes for membrane protein association. *J. Phys. Chem. B* **2017**, *121*, 3364−3375.
(54) Davis, J. P.; Norman, C.; Kobayashi, T.; Solaro, R. J.; Swartz, D. R.; Tikunova, S. B. Effects of thin and thick filament proteins on calcium binding and exchange with cardiac troponin C. *Biophys. J.* **2007**, *92*, 3195−3206.
(55) Tikunova, S. B.; Liu, B.; Swindle, N.; Little, S. C.; Gomes, A. V.; Swartz, D. R.; Davis, J. P. Effect of calcium-sensitizing mutations on calcium binding and exchange with troponin C in increasingly complex biochemical systems. *Biochemistry* **2010**, *49*, 1975−1984.
(56) Li, M. X.; Spyracopoulos, L.; Sykes, B. D. Binding of cardiac troponin-I147-163 induces a structural opening in human cardiac troponin-C. *Biochemistry* **1999**, *38*, 8289−8298.
(57) Robertson, I. M.; Sun, Y.-B.; Li, M. X.; Sykes, B. D. A structural and functional perspective into the mechanism of Ca2+-sensitizers that target the cardiac troponin complex. *J. Mol. Cell. Cardiol.* **2010**, *49*, 1031−1041.
(58) Kobayashi, T.; Solaro, R. J. Increased Ca2+ affinity of cardiac thin filaments reconstituted with cardiomyopathy-related mutant cardiac troponin I. *J. Biol. Chem.* **2006**, *281*, 13471−13477.
(59) Zhou, H.-X.; Pang, X. Electrostatic interactions in protein structure, folding, binding, and condensation. *Chem. Rev.* **2018**, *118*, 1691−1741.
(60) Schrödinger Release 2022-1. *Maestro*; Schrödinger, LLC: New York, NY, 2021.
(61) Ohio Supercomputer Center. *Ohio Supercomputer Center*; Ohio Supercomputer Center: Columbus OH, 1987.

https://doi.org/10.1021/acs.jcim.3c00388
J. Chem. Inf. Model. 2023, 63, 3534−3543